An Operando X-Ray Absorption Spectroscopy Study of a NiCu-TiO_2 Photocatalyst for H_2 Evolution

Davide Spanu,[a] Alessandro Minguzzi,[b] Sandro Recchia,[a] Fahimeh Shahvardanfard,[c] Ondřej Tomanec,[d] Radek Zboril,[d] Patrik Schmuki,[c,d,e] Paolo Ghigna,[f] and Marco Altomare[c]*

[a] Department of Science and High Technology, University of Insubria, via Valleggio 11, 22100 Como, Italy

[b] Dipartimento di Chimica, Università degli Studi di Milano, Via Golgi 19, 20133 Milan, Italy

[c] Department of Materials Science and Engineering WW4-LKO, University of Erlangen-Nuremberg, Martensstrasse 7, D-91058 Erlangen, Germany

[d] Regional Centre of Advanced Technologies and Materials, Faculty of Science, Palacky University, Olomouc, Šlechtitelů 27, 783 71 Olomouc, Czech Republic

[e] Chemistry Department, Faculty of Sciences, King Abdulaziz University, 80203 Jeddah, Saudi Arabia Kingdom

[f] Dipartimento di Chimica, Università degli Studi di Pavia, Viale Taramelli 13, 27100 Pavia, Italy

* Corresponding author. E-mail: marco.altomare@fau.de

Abstract

Cu- or Ni-decorated semiconductors represent a potential low-cost alternative to noble metal-modified photocatalysts. Even more effective are bimetallic NiCu nanoparticles, which can provide a remarkable photocatalytic H_2 evolution enhancement compared to single element Cu- or Ni-systems. A main question of such alloyed co-catalysts is their activity with respect to alteration of their elemental composition and oxidation state over reaction time. Ex-situ characterization techniques provide controversial interpretations of the co-catalytic role of the individual elements. Hypotheses such as the in-situ reduction of "native" Ni or Cu species during photocatalysis, the oxidation of metallic Cu or Ni into oxides or hydroxides, or the formation of p-n junctions or core/shell structures, have been proposed. Herein we present an operando X-ray absorption spectroscopy study of a NiCu-TiO_2 system under UV light illumination in ethanol-water solutions, *i.e.* under photocatalytic H_2 evolution conditions. The experimental approach and cell design allow for monitoring in real time chemical changes that take place in the co-catalyst under intermittent illumination, i.e. under light on-off cycles. We show that while Ni and Cu are partially oxidized in the as-formed NiCu co-catalyst (air formed surface oxides or hydroxides), and undergo partial dissolution in the liquid phase under dark conditions, such Ni and Cu oxidized and dissolved species are reduced/re-deposited as bimetallic NiCu phase at the TiO_2 surface under illumination. The dissolution/re-deposition mechanism is triggered by TiO_2 conduction band electrons. We not only prove a UV light induced healing of the NiCu co-catalyst, but also unambiguously demonstrate that the species responsible for the strongly enhanced photocatalytic H_2 evolution of NiCu nanoparticles are the metallic states of Ni and Cu.

Keywords: Solid-state dewetting, NiCu alloy nanoparticles, TiO_2 nanotubes, photocatalytic H_2 evolution, in-situ XAS

Graphical Abstract

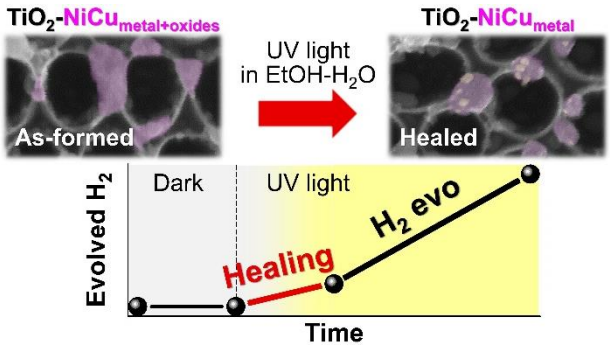

Introduction

The photocatalytic production of H_2 from water/organic mixtures is envisaged as a most promising way to generate clean energy vectors for the future.[1] With the pioneering work of Fujishima and Honda,[2] titanium dioxide (TiO_2) has become a most widely investigated semiconductor for photocatalytic and photo-electrochemical applications.[3–5] However, from a kinetic point of view, pristine TiO_2 shows performance limitations ascribed to trapping and recombination of charge carriers, these causing inefficient transfer of CB electrons to suitable precursors to react to H_2.[6]

Particularly effective for improving the performance of a photocatalyst are localized Schottky junctions, which can be formed by depositing noble metal nanoparticles (e.g. Pt, Pd or Au NPs) on the TiO_2 surface.[7–10] Noble metal NPs are highly active co-catalysts for hydrogen evolution due to their ability to act as an electron sink and transfer mediator and, particularly in the case of Pt, to provide catalytic sites for recombination of hydrogen atoms.[9,10] Their high-cost and low-abundance, however, question their use and have triggered research efforts towards the identification of alternative earth-abundant co-catalysts.[11,12] The latter can enable promising activity enhancement effects particularly when used in the form of bimetallic NPs.[11,13–16]

In this context, we have recently reported[11] on an efficient noble metal-free photocatalyst for H_2 evolution based on bimetallic NiCu NPs formed by solid-state dewetting[17,18] on TiO_2 nanotube (NT) arrays. Such NiCu-TiO_2 systems can not only exhibit a significantly higher activity compared to monometallic counterparts (Ni-TiO_2 and Cu-TiO_2) but, even more importantly, also display a photocatalytic performance approaching the values reported for Pt-TiO_2 benchmarks.[11]

The poor chemical inertness of metal co-catalysts such as Ni or Cu is perceived however as a main shortcoming. Cu or Ni co-catalysts may in fact undergo substantial chemical changes not only under ambient conditions but also during the photocatalysis. Previous work on Cu[19–26] and Ni[27–34] co-catalysts for photocatalysis shows that these metals undergo changes in their oxidation states, crystallinity, as well as particle shape and size during photocatalytic reactions. Some studies suggest the formation of Cu metal from "native" Cu oxidized species via TiO_2 photo-generated CB electrons.[19–21,26] For example, Polliotto et al.[19] propose that Cu_2O NPs are reduced to metallic Cu under illumination, and Hejazi et al.[22] observed for Cu-doped TiO_2 nanotubes the formation of metallic Cu decorations via dissolution of Cu^{2+} from the TiO_2 structure. Other reports such as that of Jung et al.[20] show that when starting from a CuO co-catalyst (Cu(II)), a reduction process that forms Cu_2O (Cu(I)) occurs. Differently, the oxidation of Cu^0 to Cu^{2+} along with the formation of core-shell NPs (metallic core and oxidized Cu^{2+} shell) was observed during gas phase photocatalytic H_2 evolution.[35] Furthermore, Irie et al. (and Dozzi and coworkers in follow up works) proposed that since the redox potential of the Cu^{2+}/Cu^{+} couple or the CB minima of crystalline CuO are less negative than the CB energy of TiO_2, Cu^{2+} species on the TiO_2 surface may capture TiO_2 CB electrons causing a consequent one-electron reduction of oxidized copper species (Cu^{2+} to Cu^{+}) meanwhile enhancing the charge carrier separation efficiency.[36,37] This effect was reported to enable visible light activation, as electrons in the VB of TiO_2 are directly transferred to the discrete energy levels of grafted Cu^{2+} species.

Controversial mechanisms are reported also for Ni. Some reports suggest that "native" Ni oxide or hydroxide are reduced by photo-generated CB electrons to metallic Ni.[27–29] For this, dissolution of oxidized Ni species precedes Ni ion reduction and photo-deposition.[31] This, in general, takes places if holes in the illuminated semiconductor are rapidly consumed by a hole

scavenger (organics e.g. methanol, ethanol etc.) and Ni decorations can trap TiO_2 CB electrons and maintain a metallic state, or undergo reduction to a metallic phase if Ni oxidized species are initially present. In this scenario, the resulting metal NPs act as co-catalyst for the hydrogen evolution reaction (HER). However, an absence of chemical changes for Ni NPs,[35] or oxidation or disproportionation reactions forming both Ni and NiO_x sites[32] or Ni/NiO_x core-shell NPs[30] were also proposed. Such NiO_x compounds or Ni/NiO_x core-shell nanostructures are reported to form in the case of overall water splitting photocatalysts investigated in pure water. In the absence of a "fast" sacrificial agent, photo-generated holes can oxidize Ni metal decorations at the semiconductor surface forming ("conditioning") in-situ a NiO_x co-catalyst for water oxidation to O_2 (oxygen evolution reaction, OER).

Besides the nature of the metal co-catalyst (noble vs. non noble) and the reaction conditions (presence of a hole scavenger), the discrepancy between such interpretations may originate from the fact that most studies were based on indirect observations from ex-situ techniques, i.e. the characterization of Cu and Ni co-catalysts was performed before and/or after photocatalysis, while chemical changes taking place during photocatalysis could not be observed in real time or were not detected at all.

Herein, we explore the chemical state of Cu and Ni in a NiCu-TiO_2 photocatalyst by a combination of ex-situ techniques (before and after photocatalysis) and operando X-ray absorption spectroscopy (XAS). We adopted a spectroscopic cell that allows for XAS measurements in fluorescence mode, under UV light illumination of the photocatalyst in water-ethanol solutions, hence allowing us to monitor the Ni and Cu chemical state in real time under photocatalytic H_2 evolution conditions. This experimental design provides solid evidence that the co-catalyst responsible for H_2 evolution is a NiCu phase, where Ni and Cu exist in their reduced metallic state.

Experimental section

Fabrication of TiO_2 nanotube arrays

Ti foils (Advent Research Materials, 0.125 mm thickness, 99.6+% purity) were degreased by sonication for 15 minutes in acetone, ethanol, and deionized water and then they were dried in a N_2 stream. The degreased Ti foils were anodized in a 3M HF/o-H_3PO_4 (Sigma-Aldrich) electrolyte at 100°C to fabricate highly ordered TiO_2 nanotube arrays. A two-electrode configuration was used for the anodic growth: the Ti foil (25 mm × 15 mm) and a Pt sheet were the working and counter electrode, respectively. The anodization experiments were performed by applying a constant voltage of 15 V (for 2 h) using a DC power supply (VLP 2403 Voltcraft). After anodization, the TiO_2 nanotube arrays supported by Ti metal substrates were rinsed with ethanol, soaked in ethanol overnight and then dried in a N_2 stream.

Metal film sputter-coating and solid-state dewetting

A plasma-sputtering machine (EM SCD 500, Leica) was used to sputter-coat Cu and Ni thin metal films on the TiO_2 nanotube arrays. A 99.90% pure Cu target (Baltic Praeparation e.K.) and a 99.98% pure Ni target (Hauner Metallische Werkstoffe) were used for the sputtering process. The applied sputtering current was 16 mA for both metals and the pressure of the sputtering chamber was set at 10^{-2} mbar of Ar. The amount of sputtered material was in-situ determined by an automated quartz crystal monitor built in the sputtering machine; the amount of deposited metal is expressed as nominal thickness of the metal film in nanometers. After sputtering, the samples were annealed at 450°C (1 h) in Ar (Ar flux = 10 L h^{-1}) to induce both dewetting of the metal films (and Ni-Cu intermixing) and crystallization of TiO_2.

Ex-situ characterization of the photocatalysts

A field-emission scanning electron microscope (FE-SEM, Hitachi S4800) and a transmission electron microscope (TITAN 60–300, FEI, USA) were used to characterize the morphology (by SEM and HAADF-TEM) and chemical composition (by EDS-TEM) of the samples. X-ray diffraction (XRD) with an X′pert Philips MPD (equipped with a Panalytical X'celerator detector) was employed to examine the crystallographic properties of the materials. The chemical composition of the samples, particularly of the co-catalyst NPs, was analyzed by X-ray photoelectron spectroscopy (XPS, PHI 5600, US) and peak positions were calibrated with respect to the C1s peak at 284.8 eV. The deconvolution of the XPS peaks was performed by using Origin 2016 software (OriginLab®, Northampton, USA) and the fitting of the signals was done by adopting symmetric Voigt profiles.

Photocatalytic measurements

Photocatalytic measurements for H_2 generation were carried out by irradiating the TiO_2-based photocatalysts in a 20 vol% ethanol-water solution in a quartz tube sealed with a gas-tight cap. As light sources we used a LED UV light (Opsytec, λ = 365 nm, beam size = 0.785 cm^2, power of 100 mW cm^{-2}).

We used ethanol as a sacrificial electron donor (or hole scavenger). Due to the lower oxidation potential of ethanol compared to water, ethanol can efficiently capture TiO_2 VB holes. This leads to ethanol oxidation (finally to CO_2) and, most importantly, limits the recombination of electron/hole pairs in TiO_2, increasing the lifetime of CB electrons and thus the overall hydrogen evolution reaction (HER) rate. The oxidation of ethanol is comparably fast and takes place likely via direct VB holes at the free TiO_2 surface.

The ethanol-water solution (kept under static conditions during the runs) and the cell head-space (volume = 3.5 mL) were purged with Ar gas for 30 min dark conditions prior to photocatalysis. The experiments lasted in average 4 hours. Ar-purging (in the dark) is needed to remove O_2 from the liquid phase and from the head space. O_2, if present, undergoes reduction to $O_2^{-\bullet}$ radicals mediated by TiO_2 CB electrons, hence limiting the H_2 evolution efficiency. In the present study, the photocatalysts were investigated by in-situ XAS experiments (outlined below) not only during photocatalysis, but also under dark conditions. In our view, there is somehow a lack of in-situ studies for photocatalytic systems although it is essential to understand the physicochemical state and morphological features of the co-catalyst before, during and after operation. That is, a better understanding of transient changes ongoing under intermittent illumination can pave the way for a more rational photocatalyst design. Perspective wise, photocatalytic systems are in fact required to operate under solar light and thus under intermittent irradiation. A photocatalyst that shows poor stability and degrade in the dark without healing under illumination is obviously not a promising material for real photocatalytic applications.

The amount of produced H_2 (accumulated in the head space of the tube during irradiation) was measured by a gas chromatograph (GCMSQO2010SE, Shimadzu) equipped with a thermal conductivity detector and a Restek micropacked Shin Carbon ST column (2 m × 0.53 mm). GC measurements were carried out at a temperature of the oven of 45°C (isothermal conditions), with the temperature of the injector set at 280°C and that of the TCD fixed at 260°C. The flow rate of the carrier gas (Ar) was 14.3 mL min^{-1}.

Operando synchrotron experiments and spectroscopic cell design

The operando XAS experiments were carried out at DESY – Petra III, P65, Hamburg, Germany. For these experiments we designed a liquid-phase cell as shown in Figure S1. The cell has a Mylar window to grant transparency for both X-rays and UV light, thus allowing X-rays collection under UV light illumination of the photocatalyst. The photocatalyst was immersed in a 20 vol% ethanol-water solution. The solution was purged with nitrogen gas (saturated with ethanol-water vapors) prior and during the entire investigation time. We used for illumination the same UV LED light source as in the photocatalytic experiments. We used a Passivated Implanted Planar Silicon (PIPS) detector that allowed for collecting a full XAS spectrum in ca. 15-20 min (depending on the energy range) and thus to perform time-resolved experiments, since the timescale of the phenomena we detected (shifts in Cu and Ni chemical state) happened to be in the order of e.g. some to a few tens of minutes. This specific cell design allows to work with a minimized thickness of the solution film in front of the sample, this to cope with the penetration depth of X-rays at the target edges (ca. 1 mm) and hence to enable an adequate amount of photons to reach the detector.

The X-ray absorption near edge structure (XANES) spectra shown in Figures 3 and 4 were obtained by subtracting the pre-edge background. The spectra were then fitted with a straight line and without any further manipulation. The quantification of the relative amount of Cu and Ni in the different oxidation states was obtained by fitting the normalized XANES spectra (absorption equals the unit at 500 eV after the edge, where the EXAFS oscillations are not visible anymore). The fitting was carried out by using proper linear combinations of normalized spectra measured for the reference compounds (Cu, Cu_2O, CuO, Ni, NiO). NiO, CuO and Cu_2O phases detected by XANES should be considered as indicative of the presence

of Ni(II), Cu(II) and Cu(I). Information such as the oxide vs. hydroxide surface composition of the co-catalyst NPs are complemented by XPS data.

Results and discussion

In the present work anodic TiO_2 NT arrays[3,4,38,39] with a short aspect ratio were employed as a photocatalytic platform due to their morphological features, i.e. their high level of self-ordering and defined periodicity that make them a suitable substrate for templated dewetting.[18,40,41]

NiCu bilayers with a nominal total thickness of 10 nm were deposited by Ar-plasma sputtering onto the TiO_2 NT substrates. Ni was sputtered directly on TiO_2 and Cu was deposited afterwards over the Ni film. Then, a thermal treatment was carried out to induce solid-state dewetting of the metal bilayer in an inert atmosphere.[42–45] Upon annealing in Ar, Ni and Cu atoms inter-diffuse forming NiCu bimetallic NPs at the semiconductor surface. The NP composition was controlled by adjusting the initial thickness of the Ni and Cu films.[11,18] As a reference, 10 nm thick Ni or Cu films were also sputter-dewetted yielding pure Ni or Cu NP decorations.

SEM images that illustrate the formation of Cu and Ni dewetted particles are shown in Figure 1a-e. Samples are named according to the co-catalyst composition: "*x*Ni*y*Cu-TiO_2", where "*x*" and "*y*" are the nominal thicknesses of the sputtered metal films expressed in nm.

We examined the particle size distribution for samples 10Ni, 5Ni5Cu and 10Cu in our previous work – see ref.[11] (Figure S3a-c therein). The average size of the dewetted metal NPs appears independent of the initial metal film composition. Ni (10 nm) and Cu (10 nm) films, as well as NiCu bilayers (5+5 nm), dewet into ~ 30-40 nm sized NPs. Compared to dewetted Ni NPs that grow relatively close to each other, dewetted Cu NPs show a slightly lower

distribution density at the TiO_2 NT surface. This may suggest that Ni and Cu exhibit different dewetting modes, due e.g. to their different melting point, surface diffusion or substrate wettability, and the dewetting behavior of NiCu bilayers may hence depend on the initial composition of the bilayer.

In line with previous work,[11,13–16,26] the photocatalytic activity of TiO_2 decorated with bimetallic NiCu NPs is substantially higher than that of monometallic counterparts (i.e. Ni-TiO_2 or Cu-TiO_2) due to the synergistic interaction between Cu and Ni (see the photocatalytic hydrogen evolution rates reported in Figure 1f). Cadenhead et al.[46] proposed that the enhanced activity of NiCu NPs is due to their bifunctional surface: the fast adsorption/recombination of H atoms at Ni centers synergizes with favorable H_2 gas desorption at adjacent Cu sites. Other authors concluded that the crucial factor is the higher work function of NiCu NPs with respect to that of Cu (4.65 eV for Cu and 5.15 eV for Ni), which can enable a more efficient electron-hole separation.[47–49] Nonetheless, these interpretations are valid only if Cu and Ni exist in the co-catalyst NPs in their metallic state.

However, as reported in the literature,[19,20,27–30,35] Ni and Cu NPs undergo significant chemical transformations not only under ambient conditions (they are susceptible to oxidation by oxygen in the environment[50,51]) but also when exposed to a reaction phase, in the dark or under illumination (e.g. during photocatalysis). As a preliminary indication of such phenomena, one can notice that, when comparing the as-prepared photocatalyst (Figure 1c-e) with a sample after 4 hours of photocatalytic activity (Figure 1g-i, samples labelled *x*Ni*y*Cu-P), some clear morphological changes for the Ni and NiCu NPs have occurred. Figure S2 shows a direct comparison of high-magnification SEM images for sample 5Ni5Cu before and after photocatalysis. The pure Cu NPs, on the contrary, appear almost unchanged.

Ex-situ XPS and XRD measurements performed prior and after photocatalytic experiments, and ex-situ as well as in-situ XAS measurements were adopted to gain relevant information on co-catalyst transformations occurring during photocatalysis – see supporting information (page S2 and S3) for further discussion.

The XRD patterns (shown in Figure 2a-b) prove that as-prepared 10Cu-TiO_2, 10Ni-TiO_2 and 5Ni5Cu-TiO_2 are decorated with dewetted pure Cu, pure Ni and alloyed NiCu NPs, respectively. The peaks observed in the pattern of sample 10Cu-TiO_2 at 43.3° and 50.4° can be indexed to the Cu 111 and Cu 200 reflections,[52] whereas the presence of Ni in sample 10Ni-TiO_2 is confirmed by the presence of the peak at 44.4° that can be assigned to the Ni 111 reflection.[53] Dewetted-alloyed NiCu NPs can be identified in sample 5Ni5Cu-TiO_2 by the presence of the peak at 43.9°, i.e. NiCu 111 reflection, which falls between the pure Cu and pure Ni 111 reflections, hence fitting well to Vegard´s law.[16,54] A comparison of XRD patterns (Figure 2a-b) recorded for fresh (continuous lines) and tested materials (dotted lines) reveals that the crystallographic features of Ni, Cu and NiCu NPs are not significantly influenced by the photocatalytic process, i.e. the corresponding diffractograms are virtually identical and no crystalline Ni or Cu oxide phase could be detected. Moreover, for NiCu NPs no peaks of pure Ni or Cu metal phase can be seen after photocatalysis.

The peaks at 25.3° and 27.4° confirm, for samples 10Ni-TiO_2 and 5Ni5Cu-TiO_2, that the NTs are composed of anatase TiO_2, with minor contents of rutile phase. Such peaks can be attributed to the 101 and 110 reflections of anatase and rutile TiO_2 phases, respectively. Differently, the XRD pattern of sample 10Cu-TiO_2 shows rutile TiO_2 to be the dominant phase. This is in line with what observed in previous work[11] and may suggest that, during thermal dewetting, pure Cu films better stabilize the TiO_2 rutile phase with respect to the

anatase phase.[55,56] Besides, the peaks at 38.5° and 40.2° present for every sample can be assigned to the Ti metal substrate.

The Ni2p and Cu2p XPS spectra (reported in Figure 2c-f and Figure S3) reveal the presence of large amounts of surface oxides/hydroxide species in all as-prepared photocatalysts (relative Ni and Cu compositions with a speciation that is summarized in Figure 2g and Table S1). By fitting the XPS signals of sample 5Ni5Cu-TiO_2 (Figure 2c,d) it is possible to identify the bands at 851.9 and 932.4 eV that can be attributed to Ni and Cu metals, respectively. The peaks at higher binding energies are ascribed to the presence of Ni and Cu oxides/hydroxides.[57–60] The high degree of surface oxidation is likely due to sample storage under atmospheric conditions (air formed oxidized metal species).

Interestingly, the comparison of Cu and Ni speciation before and after photocatalysis (see Figure 2g) shows that the relative amount of metal significantly increases after photocatalytic H_2 evolution, at the expense of the content of oxide/hydroxide species. This trend may suggest, for all the samples (10Ni- 10Cu- and 5Ni5Cu-TiO_2), the occurrence of a partial reduction of Ni and Cu NPs under photocatalytic conditions. Nonetheless, the content of Ni and Cu oxides/hydroxides after photocatalysis is still significant.

To evaluate if the relatively high content of oxygen in the photocatalyst may originate from adsorbed oxidized species formed by ethanol oxidation during photocatalysis, we measured, for the different photocatalysts, XPS spectra in the C 1s region before (as-formed samples) and after photocatalysis. The spectra are shown in Figure S4, while quantitative data are summarized in Table S2. We found no evident correlation between the carbon content results and the amount of oxidized Ni and Cu compounds after photocatalysis. The C content is always about 3 at% or lower, and appears to decrease or to remain unaffected after photocatalysis. Hence, to account for the large content of Ni and Cu oxidized species

observed by XPS for the samples after photocatalysis, we propose that even if at the end of the photocatalytic experiments Ni and Cu are mainly present in their metallic state, as determined by the operando XAS experiments detailed below, the co-catalyst NPs may undergo partial oxidation when the samples are no longer illuminated and are transferred under ambient conditions to the XPS chamber.

Energy dispersive spectroscopy-transmission electron microscopy (EDS-TEM) data (Figure 2h-j) show that NPs dewetted at the TiO_2 NT surface from NiCu bilayers feature a partially mixed Ni-Cu composition (Figure 2i).[11,46,61] Apparently, Cu is mostly exposed to the environment while Ni seats in direct contact with the TiO_2 phase, i.e. mirroring the sputtering sequence. Additionally, oxygen is distributed over the entire NP surface (Figure 2j), but its concentration seems to be higher in the outermost ~ 5 nm of the NP and at the Ni-rich zones. The presence of the outer thin oxide layer "wrapping" the Cu-rich zone, as mentioned above, may be explained by sample exposure to ambient conditions,[50,51] whereas the oxygen distribution over the Ni-rich region can be ascribed to a strong interaction between Ni and TiO_2 during dewetting.[62]

Summing up, ex-situ XRD, XPS and EDS-TEM analysis evidence for the co-catalyst NPs the presence of oxidized surface Cu and Ni species with a metallic NP core. Moreover, the data apparently suggest that the content of metallic Cu and Ni relative to that of their oxides is higher after photocatalysis than in the as-formed samples.

For these reasons, we used a spectroscopic cell (Figure S1) for operando XAS measurements to monitor in real time the co-catalyst evolution during photocatalysis. The cell allows to work with a thin liquid solution film (< 1 mm-thick) in front of the sample. The cell design and experimental conditions reproduce as accurately as possible the working conditions adopted for the photocatalytic H_2 evolution experiments.

Prior to the operando measurements, the composition of the as-prepared photocatalysts was assessed in order to obtain a reference of the starting Ni and Cu speciation for all the samples. The samples were measured in air and in the dark. Figures 3a,b show the Cu and Ni K-edge spectra of as-prepared 10Cu, 10Ni and 5Ni5Cu samples (the spectra of standards for the different oxidation states are also shown for comparison). All the spectra of the standards show the expected chemical shift, i.e. the X-ray absorption edge is shifted to higher energy for higher oxidation states of the photo-absorber. In addition, the spectra of metallic Cu and Ni display a characteristic peak of the absorption coefficient at low energy (~ 8983 and ~ 8333 eV, respectively) due to transitions from the 1*s* core level to bound empty levels in the conduction band of the metals. At both the Cu and Ni K-edges, the spectra of the 5Ni5Cu sample show remarkable differences if compared to those of 10Cu and 10Ni. In particular, for 5Ni5Cu, the peak at lower energy displays a lower intensity at the Ni K-edge and a larger intensity at the Cu K-edge, demonstrating that 5Ni5Cu contains a larger fraction of metallic Cu and a lower fraction of metallic Ni if compared to the 10Ni and 10Cu parent materials. For a more precise quantitative assessment of the phase composition, linear combination fittings by using the standard spectra were performed at both edges for all the samples. An example showing the fit quality is shown in the Supplementary Information (Figure S5). The resulting compositions are compiled in Figure 3a,b and in Table S3.

Afterwards, we carried out a series of operando XAS experiments for the most active photocatalyst, i.e. 5Ni5Cu-TiO_2. As a first experiment, the fresh photocatalyst was immersed in a degassed water-ethanol solution in the cell. The spectra at both Ni and Cu K-edges were acquired at subsequent times under dark conditions (no UV light). The results are shown in Figure 3c,d (see also normalized spectra in Figure S6).

At the Cu K-edge, the spectra show: i) a disappearance of the peak at 8983 eV, that indicates a reduction of the fraction of Cu in the metallic state, ii) a progressive decrease of the value of the absorption coefficient (edge jump), which is related to the amount of sample in the X-ray beam, and iii) a slow shift of the absorption edge towards higher energy, that is indicative of a slight increase in the oxidation state of Cu. Quantification of this last phenomenon can be obtained by using the same linear combination fitting procedure as described above. The results are summarized in Table S4. The progressive decrease of the amount of sample in the X-ray beam (reduction of edge height) indicates dissolution of Cu (species). The geometry of the operando cell used for these experiments is such that the largest portion of the liquid phase is behind the sample in the back of the cell, i.e. upon dissolution, the metal (Cu or Ni) ions reside behind the sample, thus outside the optical path of the X-ray and cannot therefore contribute to the detected fluorescence signal. In other words, with this configuration, the collected signal mainly originates from Cu and Ni species close or at the TiO_2 surface.

The kinetics of the Cu dissolution process can be estimated by evaluating the difference of the absorption coefficient ($\Delta\mu$) at 9020 eV measured for the sample in air (black curve in Figure 3c) and for the same sample in solution in the dark at different exposure times. The $1-(\Delta\mu/\mu)$ values (which provide a straightforward indication of the Cu co-catalyst loss due to dissolution) are plotted in Figure 3e as a function of time of exposure to the solution and prove that Cu dissolution is a slow process that continuously proceeds over the entire investigation time of 120 minutes.

For what concerns Ni, by following an approach similar to that used for Cu, a comparable dissolution process can be measured, i.e. reduction of the absorption coefficient at 8370 eV. The remarkable difference is that here the dissolution process stops after 20 minutes of

exposure to the solution as shown by the trend of $1-(\Delta\mu/\mu)$ values in Figure 3e (blue dots). Moreover, it is noteworthy that the hump at 8333 eV is increasing in relative amplitude, leading to the conclusion that the mean oxidation state of Ni is decreasing and that a significant fraction of Ni is in the metallic state after exposure to the solution (see Table S4 for quantification).

The EDS-TEM image in Figure 2i may suggest that the morphology of the dewetted NiCu NPs is such that the Cu-rich part "protects" most of the Ni-rich side, thus explaining the long-lasting, progressive dissolution of Cu upon exposure to the liquid phase. In other words, based on data in Figures 3c-e and Table S4, one can conclude that i) after synthesis, the NiCu NPs undergo surface oxidation when air-exposed; ii) in ethanol-water, the dissolution of surface Cu oxides exposes fresh Cu metal to further oxidation and consequent partial dissolution, iii) the dissolution of Ni oxides occurs to a comparably small extent (likely because the exposed Ni phase is less), and iv) the Ni phase left behind on the TiO_2 NTs and protected by Cu is not corroded.

In a following experiment, after sample exposure to the ethanol-water mixture under dark conditions, the illumination was switched on (UV light, 365 nm) and spectra were recorded at the Cu and Ni K-edges. The results are shown in Figure 4a,b (see also normalized spectra in Figure S6).

At both edges, an increase of the absorption coefficient is detected after the first 20 minutes of illumination, and thereafter μ remains constant. This leads to the conclusion that during this period a photo-induced re-deposition of both Cu and Ni from the solution takes place. In addition, the increase in amplitude of the peaks at 8983 and 8333 eV with increasing time demonstrates that Cu and Ni are in the metallic state when re-depositing on the TiO_2 NT surface. Note that, as evident from Figure 4c,d and Table S5, already after 40 minutes under

illumination, Cu is entirely metallic (100%) while Ni is almost all in the metallic state (85%). This proves that metallic Cu and Ni are the species present under photocatalytic H_2 evolution conditions, that is, a bimetallic NiCu phase (and not Ni or Cu oxides or hydroxides) is responsible for the co-catalytic effect enabling H_2 evolution.[26] This result, as discussed in the introduction for Ni based co-catalysts, may also be caused by the presence of a hole scavenger (ethanol) in the reaction phase – that is, Ni may undergo reduction to its metallic state when in the presence of a hole scavenger (as in our experiments) and act therefore as a co-catalyst for H_2 evolution, while in pure water (no hole scavenger) it may undergo oxidation forming a Ni/NiO_x phase, operating hence in an oxidized state to promote the O_2 evolution reaction.[30,32]

Operando XAS results for reference $Cu\text{-}TiO_2$ and $Ni\text{-}TiO_2$ structures are shown in Figure S7, Table S6 and Table S7. The data for $Cu\text{-}TiO_2$ (Figure S7a, Table S6) and $Ni\text{-}TiO_2$ structures (Figure S7b, Table S7) show a behavior analogous to that observed for $NiCu\text{-}TiO_2$: the as-formed co-catalysts (Cu or Ni NPs) show a sizeable content of oxidizes species, likely due to air formed oxides and hydroxides at the NP surface as shown by ex-situ XPS and XAS data of the as-formed samples (Figure S3a,b and 3a,b, respectively). However, under illumination, Ni and Cu oxidized species undergo reduction to Cu and Ni metallic states in few tens of minutes (Tables S6 and S7). Hence, under UV light illumination and under photocatalytic H_2 evolution conditions, not only the bimetallic NiCu co-catalyst but also Ni and Cu NPs on TiO_2 are active in their metallic state and can promote H_2 evolution via a Schottky junction type mechanism (i.e. CB electron trapping and transfer to H^+ for H_2 evolution).

In heterogeneous catalysis, operando XAS studies are commonly carried out, e.g. to investigate catalysts (in the form of powder pellets or thin films) typically in gas phase reaction spectroscopic cells.[35,63–65] The adoption of such experimental configuration was

reported for example to study the oxidation state of Pt in Pt-TiO_2 photocatalysts.[66] More relevant to our work is a recent report by Munoz-Batista and co-workers,[35] who used a comparable approach to investigate in a gas phase cell a NiCu-TiO_2 photocatalyst powder for H_2 evolution.[35] When the photocatalyst was exposed to methanol-water vapors, they observed that Cu is under dark conditions in its metallic state, while oxidizes to Cu(II) under illumination. On the contrary, Ni was found to be in an oxidized Ni(II) state, and negligible changes of its oxidation state took place when switching from dark to light conditions. The conclusions by Munoz-Batista et al. differ significantly from our findings but the reason is simply that our experimental conditions, i.e. in ethanol-water solutions, allow for dissolution and re-deposition while this of course is not possible in a vapor phase process.

The interpretation of our XAS results is also confirmed by an experiment carried out as follows: a fresh 5Ni5Cu-TiO_2 sample was placed in the photocatalytic cell and the composition of the cell head space was sampled and analysed by gas-chromatography to determine the amount of evolved H_2 (i) after 2 hours during which the photocatalyst was kept in the dark; (ii) after another 2 hours of illumination; and (iii) after a further illumination time of 4 hours.

The H_2 evolution results are compiled in Figure 4e. After 2 hours under dark conditions (i), no significant amount of hydrogen could be detected. Based on XAS data, during this period (i) Cu and Ni species are proved to partially dissolve.

Hydrogen evolution was clearly observed after 2 (ii) and 6 h (iii) of UV light illumination. Nevertheless, the extrapolated H_2 evolution rates for these two illumination periods appear substantially different, i.e. 4.9 μL h^{-1} cm^{-2} in the first 2 hours and 7.4 μL h^{-1} cm^{-2} in the following 4 hours of illumination. The lower H_2 evolution rate observed during period (ii) is likely because TiO_2 CB electrons are partially consumed to reduce (photo-deposit) Cu and Ni

ions in the liquid phase. The suboptimum H_2 evolution rate can also be ascribed to a non-optimized co-catalyst composition.

It is important to point out that the H_2 evolution rate measured under illumination in the last 4 hours is virtually identical to that measured when illuminating a fresh photocatalyst that remained in the ethanol-water in the dark for only 30 minutes (for Ar purging and O_2 removal – see Experimental). These results suggest that a short illumination time (tens of minutes of illumination based on XAS data) allows the photocatalyst to recover its photo-activity due to a light induced conditioning ("healing") process where Cu and Ni ions in the ethanol-water solution undergo photo-deposition at the catalyst surface. This conditioning effect is also visible from the SEM images of the sample 5Ni5Cu-TiO_2 after photocatalysis (cf. Figures 1g and 4f with 1c and see direct comparison in Figure S2): one can see the photo-induced Ni and Cu re-deposition process forming small protrusions (a few nm sized, circled in purple in Figure 4f) on the bimetallic NPs at the TiO_2 surface. The fact that these deposits are found only at the surface of the dewetted NPs (and not directly on TiO_2), suggests that during illumination:

- First, oxides or hydroxides of Cu and Ni in the co-catalyst NPs on TiO_2 are converted to their metallic state, leading to metallic NiCu NPs;
- The NiCu NPs act then as cathodic sites, i.e. electron trap sites, that lead to photo-reduction of Ni and Cu ions present in the liquid phase due to dissolution in the previous dark period; such Ni and Cu ions deposit in their metallic state on the bimetallic NPs at the photocatalyst surface;
- Photocatalysis proceeds at highest rates when photo-deposition of Cu and Ni is completed, and the H_2 evolution is enabled by NiCu NPs where Ni and Cu are in their metallic state.

The XRD data in Figure 2b suggest that such re-deposition does not alter the bimetallic nature of the NiCu NPs, i.e. no evident formation of pure Ni or Cu phase seem to take place.

The data, overall, provide thus an in-situ evidence that the NiCu co-catalyst NPs (but also monometallic Ni and Cu NPs) operate in a metallic state and promote H_2 evolution via a Schottky junction type effect. For the highly active NiCu co-catalyst, which outperforms single element Cu or Ni systems, a crucial factor is the higher work function of NiCu NPs with respect to that of pure Cu (4.65 eV for Cu and 5.15 eV for Ni) as ascribed to the incorporation of Ni to Cu. This can improve the electron-hole separation (due to a higher Schottky barrier) and enable a more efficient electron transfer for H_2 evolution.[47–49] Moreover, the enhanced activity of NiCu NPs can be also due to their bifunctional surface, i.e. due to a fast H atom adsorption/recombination at surface Ni sites that synergizes with a more favorable H_2 gas desorption at adjacent surface Cu sites.[46] Note that these two mechanisms can be proposed exclusively because we prove the metallic nature of the active NiCu co-catalyst state.

Conclusions

We present an operando X-ray absorption spectroscopy study of a nanostructured NiCu-TiO_2 photocatalyst. For this, we use a liquid-phase spectroscopic cell for XAS measurements in fluorescence mode to monitor in real time the NiCu co-catalyst composition and oxidation state during photocatalytic H_2 generation from ethanol-water mixtures. We demonstrate that under illumination, oxidized Ni and Cu species (native oxides and hydroxides at the co-catalyst surface) are reduced to a bimetallic NiCu phase via dissolution/re-deposition. We observe light induced conditioning of the NiCu nanoparticles (“healing”) that causes an increase of the H_2 evolution activity. The results clearly show that elements in the metallic

state in the co-catalyst are responsible for the enhanced photocatalytic H_2 generation observed for this catalyst.

Overall, our study demonstrates that, despite an apparent thermodynamic instability of non-noble co-catalysts such as Ni, Cu and bimetallic NiCu NPs, healing effects under operation conditions “repair” such instability.

Besides, the present work highlights the importance of in-situ techniques to investigate in operando the photocatalyst chemical nature, its dynamics, and transient changes under intermittent illumination. The results can be relevant not only for the mechanistic understanding but also for future design of efficient earth abundant metal co-catalysts.

Conflicts of interest

The authors declare no conflict of interest.

Supporting Information

Photograph of the spectroscopic cell and experimental setup employed for the operando XAS experiments; Additional SEM, XPS and XAS data.

Acknowledgements

M.A., F.S. and P.S. would like to acknowledge ERC, DFG and the DFG cluster of excellence EAM for financial support, as well as H. Hildebrand, A. Friedrich, A. Knoop and U. Marten-Jahns for technical help. M.A. acknowledges the financial support from the Emerging Talents Initiative ETI (ETI2018/2_Tech_11) provided by the FAU Friedrich-Alexander University Erlangen-Nuremberg, Germany. M.A., P.G. and A.M. acknowledge DESY (Hamburg, Germany), a member of the Helmholtz Association HGF, for the provision

of experimental facilities. Parts of this research were carried out at DESY – PETRA III (Project I-20190283) and we would like to thank Dr. Edmund Welter for technical assistance in using the photon beamline P65. The research leading to this result has been supported also by the project CALIPSOplus under the Grant Agreement 730872 from the EU Framework Programme for Research and Innovation HORIZON 2020. A.M. acknowledges "Piano di Sostegno alla Ricerca, Università degli Studi di Milano". P.G. acknowledges financial support by MIUR trough the grant “PRIN 2017, 2017KKP5ZR, MOSCATo”. D.S. and S.R. gratefully acknowledge financial support from MIUR.

References

(1) Christoforidis, K. C.; Fornasiero, P. Photocatalytic Hydrogen Production: A Rift into the Future Energy Supply. *ChemCatChem* **2017**, *9* (9), 1523–1544.

(2) Fujishima, A.; Honda, K. Electrochemical Photolysis of Water at a Semiconductor Electrode. *Nature* **1972**, *238* (5358), 37–38.

(3) Roy, P.; Berger, S.; Schmuki, P. TiO2 Nanotubes: Synthesis and Applications. *Angew. Chemie Int. Ed.* **2011**, *50* (13), 2904–2939.

(4) Lee, K.; Mazare, A.; Schmuki, P. One-Dimensional Titanium Dioxide Nanomaterials: Nanotubes. *Chem. Rev.* **2014**, *114* (19), 9385–9454.

(5) Paramasivam, I.; Jha, H.; Liu, N.; Schmuki, P. A Review of Photocatalysis Using Self-Organized TiO 2 Nanotubes and Other Ordered Oxide Nanostructures. *Small* **2012**, *8* (20), 3073–3103.

(6) Qian, R.; Zong, H.; Schneider, J.; Zhou, G.; Zhao, T.; Li, Y.; Yang, J.; Bahnemann, D. W.; Pan, J. H. Charge Carrier Trapping, Recombination and Transfer during TiO2 Photocatalysis: An Overview. *Catal. Today* **2019**, *335*, 78–90.

(7) Bamwenda, G. R.; Tsubota, S.; Kobayashi, T.; Haruta, M. Photoinduced Hydrogen Production from an Aqueous Solution of Ethylene Glycol over Ultrafine Gold Supported on TiO2. *J. Photochem. Photobiol. A Chem.* **1994**, *77* (1), 59–67.

(8) Bamwenda, G. R.; Tsubota, S.; Nakamura, T.; Haruta, M. Photoassisted Hydrogen Production from a Water-Ethanol Solution: A Comparison of Activities of Au-TiO2 and Pt-TiO2. *J. Photochem. Photobiol. A Chem.* **1995**, *89* (2), 177–189.

(9) Naldoni, A.; D'Arienzo, M.; Altomare, M.; Marelli, M.; Scotti, R.; Morazzoni, F.; Selli, E.; Dal Santo, V. Pt and Au/TiO2 Photocatalysts for Methanol Reforming: Role of Metal Nanoparticles in Tuning Charge Trapping Properties and Photoefficiency. *Appl. Catal. B Environ.* **2013**, *130–131*, 239–248.

(10) Chiarello, G. L.; Aguirre, M. H.; Selli, E. Hydrogen Production by Photocatalytic Steam Reforming of Methanol on Noble Metal-Modified TiO2. *J. Catal.* **2010**, *273* (2), 182–190.

(11) Spanu, D.; Recchia, S.; Mohajernia, S.; Tomanec, O.; Kment, Š.; Zboril, R.; Schmuki, P.; Altomare, M. Templated Dewetting–Alloying of NiCu Bilayers on TiO 2 Nanotubes Enables Efficient Noble-Metal-Free Photocatalytic H 2 Evolution. *ACS Catal.* **2018**, *8* (6), 5298–5305.

(12) Kumaravel, V.; Mathew, S.; Bartlett, J.; Pillai, S. C. Photocatalytic Hydrogen Production Using Metal Doped TiO 2 : A Review of Recent Advances. *Appl. Catal. B Environ.* **2019**, *244* (September 2018), 1021–1064.

(13) Riaz, N.; Chong, F. K.; Man, Z. B.; Sarwar, R.; Farooq, U.; Khan, A.; Khan, M. S. Preparation, Characterization and Application of Cu–Ni/TiO 2 in Orange II Photodegradation under Visible Light: Effect of Different Reaction Parameters and Optimization. *RSC Adv.* **2016**, *6* (60), 55650–55665.

(14) Tian, H.; Kang, S.-Z.; Li, X.; Qin, L.; Ji, M.; Mu, J. Fabrication of an Efficient Noble Metal-Free TiO2-Based Photocatalytic System Using Cu–Ni Bimetallic Deposit as an Active Center of H2 Evolution from Water. *Sol. Energy Mater. Sol. Cells* **2015**, *134*, 309–317.

(15) Yamada, Y.; Shikano, S.; Fukuzumi, S. Correction: Ni–Cu Alloy Nanoparticles Loaded on Various Metal Oxides Acting as Efficient Catalysts for Photocatalytic H 2 Evolution. *RSC Adv.* **2015**, *5* (59), 47997.

(16) Lin, Z.; Li, J.; Li, L.; Yu, L.; Li, W.; Yang, G. Manipulating the Hydrogen Evolution

Pathway on Composition-Tunable CuNi Nanoalloys. *J. Mater. Chem. A* **2017**, *5* (2), 773–781.
(17) Thompson, C. V. Solid-State Dewetting of Thin Films. *Annu. Rev. Mater. Res.* **2012**, *42* (1), 399–434.
(18) Altomare, M.; Nguyen, N. T.; Schmuki, P. Templated Dewetting: Designing Entirely Self-Organized Platforms for Photocatalysis. *Chem. Sci.* **2016**, *7* (12), 6865–6886.
(19) Polliotto, V.; Livraghi, S.; Krukowska, A.; Dozzi, M. V.; Zaleska-Medynska, A.; Selli, E.; Giamello, E. Copper-Modified TiO2 and ZrTiO4: Cu Oxidation State Evolution during Photocatalytic Hydrogen Production. *ACS Appl. Mater. Interfaces* **2018**, *10* (33), 27745–27756.
(20) Jung, M.; Hart, J. N.; Scott, J.; Ng, Y. H.; Jiang, Y.; Amal, R. Exploring Cu Oxidation State on TiO 2 and Its Transformation during Photocatalytic Hydrogen Evolution. *Appl. Catal. A Gen.* **2016**, *521*, 190–201.
(21) Sinatra, L.; LaGrow, A. P.; Peng, W.; Kirmani, A. R.; Amassian, A.; Idriss, H.; Bakr, O. M. A Au/Cu 2 O–TiO 2 System for Photo-Catalytic Hydrogen Production. A Pn-Junction Effect or a Simple Case of in Situ Reduction? *J. Catal.* **2015**, *322*, 109–117.
(22) Hejazi, S.; Mohajernia, S.; Wu, Y.; Andryskova, P.; Zoppellaro, G.; Hwang, I.; Tomanec, O.; Zboril, R.; Schmuki, P. Intrinsic Cu Nanoparticle Decoration of TiO2 Nanotubes: A Platform for Efficient Noble Metal Free Photocatalytic H2 Production. *Electrochem. commun.* **2019**, *98* (November 2018), 82–86.
(23) Montoya, A. T.; Gillan, E. G. Enhanced Photocatalytic Hydrogen Evolution from Transition-Metal Surface-Modified TiO $_2$. *ACS Omega* **2018**, *3* (3), 2947–2955.
(24) Gombac, V.; Sordelli, L.; Montini, T.; Delgado, J. J.; Adamski, A.; Adami, G.; Cargnello, M.; Bernal, S.; Fornasiero, P. CuO x −TiO 2 Photocatalysts for H 2 Production from Ethanol and Glycerol Solutions †. *J. Phys. Chem. A* **2010**, *114* (11), 3916–3925.
(25) Barreca, D.; Fornasiero, P.; Gasparotto, A.; Gombac, V.; Maccato, C.; Montini, T.; Tondello, E. The Potential of Supported Cu 2 O and CuO Nanosystems in Photocatalytic H 2 Production. *ChemSusChem* **2009**, *2* (3), 230–233.
(26) Majeed, I.; Nadeem, M. A.; Hussain, E.; Waterhouse, G. I. N.; Badshah, A.; Iqbal, A.; Nadeem, M. A.; Idriss, H. On the Synergism between Cu and Ni for Photocatalytic Hydrogen Production and Their Potential as Substitutes of Noble Metals. *ChemCatChem* **2016**, *8* (19), 3146–3155.
(27) Schubert, J. S.; Popovic, J.; Haselmann, G. M.; Nandan, S. P.; Wang, J.; Giesriegl, A.; Cherevan, A. S.; Eder, D. Immobilization of Co, Mn, Ni and Fe Oxide Co-Catalysts on TiO 2 for Photocatalytic Water Splitting Reactions . *J. Mater. Chem. A* **2019**, *7* (31), 18568–18579.
(28) Chen, X.; Xiong, J.; Shi, J.; Xia, S.; Gui, S.; Shangguan, W. Roles of Various Ni Species on TiO2 in Enhancing Photocatalytic H2 Evolution. *Front. Energy* **2019**, *13* (4), 684–690.
(29) Indra, A.; Menezes, P. W.; Kailasam, K.; Hollmann, D.; Schröder, M.; Thomas, A.; Brückner, A.; Driess, M. Nickel as a Co-Catalyst for Photocatalytic Hydrogen Evolution on Graphitic-Carbon Nitride (Sg-CN): What Is the Nature of the Active Species? *Chem. Commun.* **2016**, *52* (1), 104–107.
(30) Han, K.; Kreuger, T.; Mei, B.; Mul, G. Transient Behavior of Ni@NiO x Functionalized SrTiO3 in Overall Water Splitting. *ACS Catal.* **2017**, *7* (3), 1610–1614.
(31) Chen, W.-T.; Chan, A.; Sun-Waterhouse, D.; Moriga, T.; Idriss, H.; Waterhouse, G. I. N. Ni/TiO2: A Promising Low-Cost Photocatalytic System for Solar H2 Production

from Ethanol–Water Mixtures. *J. Catal.* **2015**, *326*, 43–53.
(32) Townsend, T. K.; Browning, N. D.; Osterloh, F. E. Overall Photocatalytic Water Splitting with NiOx–SrTiO3 – a Revised Mechanism. *Energy Environ. Sci.* **2012**, *5* (11), 9543.
(33) Zhang, L.; Liu, Q.; Aoki, T.; Crozier, P. A. Structural Evolution during Photocorrosion of Ni/NiO Core/Shell Cocatalyst on TiO 2. *J. Phys. Chem. C* **2015**, *119* (13), 7207–7214.
(34) Mei, B.; Han, K.; Mul, G. Driving Surface Redox Reactions in Heterogeneous Photocatalysis: The Active State of Illuminated Semiconductor-Supported Nanoparticles during Overall Water-Splitting. *ACS Catal.* **2018**, *8* (10), 9154–9164.
(35) Muñoz-Batista, M. J.; Motta Meira, D.; Colón, G.; Kubacka, A.; Fernández-García, M. Phase-Contact Engineering in Mono- and Bimetallic Cu-Ni Co-Catalysts for Hydrogen Photocatalytic Materials. *Angew. Chemie - Int. Ed.* **2018**, *57* (5), 1199–1203.
(36) Dozzi, M. V.; Chiarello, G. L.; Pedroni, M.; Livraghi, S.; Giamello, E.; Selli, E. High Photocatalytic Hydrogen Production on Cu(II) Pre-Grafted Pt/TiO 2. *Appl. Catal. B Environ.* **2017**, *209*, 417–428.
(37) Irie, H.; Kamiya, K.; Shibanuma, T.; Miura, S.; Tryk, D. A.; Yokoyama, T.; Hashimoto, K. Visible Light-Sensitive Cu(II)-Grafted TiO 2 Photocatalysts: Activities and X-Ray Absorption Fine Structure Analyses. *J. Phys. Chem. C* **2009**, *113* (24), 10761–10766.
(38) Yoo, J. E.; Lee, K.; Altomare, M.; Selli, E.; Schmuki, P. Self-Organized Arrays of Single-Metal Catalyst Particles in TiO 2 Cavities: A Highly Efficient Photocatalytic System. *Angew. Chemie Int. Ed.* **2013**, *52* (29), 7514–7517.
(39) Riboni, F.; Nguyen, N. T.; So, S.; Schmuki, P. Aligned Metal Oxide Nanotube Arrays: Key-Aspects of Anodic TiO2 Nanotube Formation and Properties. *Nanoscale Horiz.* **2016**, *1* (6), 445–466.
(40) Spanu, D.; Recchia, S.; Mohajernia, S.; Schmuki, P.; Altomare, M. Site-Selective Pt Dewetting on WO3-Coated TiO2 Nanotube Arrays: An Electron Transfer Cascade-Based H2 Evolution Photocatalyst. *Appl. Catal. B Environ.* **2018**, *237*, 198–205.
(41) Altomare, M.; Nguyen, N. T.; Hejazi, S.; Schmuki, P. A Cocatalytic Electron-Transfer Cascade Site-Selectively Placed on TiO 2 Nanotubes Yields Enhanced Photocatalytic H 2 Evolution. *Adv. Funct. Mater.* **2018**, *28* (2), 1704259.
(42) Yoo, J.; Altomare, M.; Mokhtar, M.; Alshehri, A.; Al-Thabaiti, S. A.; Mazare, A.; Schmuki, P. Photocatalytic H 2 Generation Using Dewetted Pt-Decorated TiO 2 Nanotubes: Optimized Dewetting and Oxide Crystallization by a Multiple Annealing Process. *J. Phys. Chem. C* **2016**, *120* (29), 15884–15892.
(43) Nguyen, N. T.; Altomare, M.; Yoo, J. E.; Taccardi, N.; Schmuki, P. Noble Metals on Anodic TiO2 Nanotube Mouths: Thermal Dewetting of Minimal Pt Co-Catalyst Loading Leads to Significantly Enhanced Photocatalytic H 2 Generation. *Adv. Energy Mater.* **2016**, *6* (2), 1501926.
(44) Nguyen, N. T.; Altomare, M.; Yoo, J.; Schmuki, P. Efficient Photocatalytic H2 Evolution: Controlled Dewetting-Dealloying to Fabricate Site-Selective High-Activity Nanoporous Au Particles on Highly Ordered TiO 2 Nanotube Arrays. *Adv. Mater.* **2015**, *27* (20), 3208–3215.
(45) Nguyen, N. T.; Yoo, J.; Altomare, M.; Schmuki, P. "Suspended" Pt Nanoparticles over TiO 2 Nanotubes for Enhanced Photocatalytic H 2 Evolution. *Chem. Commun.* **2014**, *50* (68), 9653.
(46) Cadenhead, D. A.; Wagner, N. J. Low-Temperature Hydrogen Adsorption on Copper-

Nickel Alloys. *J. Phys. Chem.* **1968**, *72* (8), 2775–2781.
(47) Ishii, R.; Matsumura, K.; Sakai, A.; Sakata, T. Work Function of Binary Alloys. *Appl. Surf. Sci.* **2001**, *169–170*, 658–661.
(48) Pašti, I.; Mentus, S. Electronic Properties of the PtxMe1−x/Pt(111) (Me=Au, Bi, In, Pb, Pd, Sn and Cu) Surface Alloys: DFT Study. *Mater. Chem. Phys.* **2009**, *116* (1), 94–101.
(49) Shiraishi, Y.; Sakamoto, H.; Sugano, Y.; Ichikawa, S.; Hirai, T. Pt–Cu Bimetallic Alloy Nanoparticles Supported on Anatase TiO 2 : Highly Active Catalysts for Aerobic Oxidation Driven by Visible Light. *ACS Nano* **2013**, *7* (10), 9287–9297.
(50) Keil, P.; Lützenkirchen-Hecht, D.; Frahm, R. Investigation of Room Temperature Oxidation of Cu in Air by Yoneda-XAFS. In *AIP Conference Proceedings*; AIP, 2007; Vol. 882, pp 490–492.
(51) Wang, C.-M.; Baer, D. R.; Bruemmer, S. M.; Engelhard, M. H.; Bowden, M. E.; Sundararajan, J. A.; Qiang, Y. Microstructure of the Native Oxide Layer on Ni and Cr-Doped Ni Nanoparticles. *J. Nanosci. Nanotechnol.* **2011**, *11* (10), 8488–8497.
(52) Wu, S.-H.; Chen, D.-H. Synthesis of High-Concentration Cu Nanoparticles in Aqueous CTAB Solutions. *J. Colloid Interface Sci.* **2004**, *273* (1), 165–169.
(53) Davar, F.; Fereshteh, Z.; Salavati-Niasari, M. Nanoparticles Ni and NiO: Synthesis, Characterization and Magnetic Properties. *J. Alloys Compd.* **2009**, *476* (1–2), 797–801.
(54) De Rogatis, L.; Montini, T.; Lorenzut, B.; Fornasiero, P. NixCuy/Al2O3 Based Catalysts for Hydrogen Production. *Energy Environ. Sci.* **2008**, *1* (4), 501–509.
(55) Sahu, M.; Biswas, P. Single-Step Processing of Copper-Doped Titania Nanomaterials in a Flame Aerosol Reactor. *Nanoscale Res. Lett.* **2011**, *6* (1), 441.
(56) Francisco, M. S. P.; Mastelaro, V. R. Inhibition of the Anatase−Rutile Phase Transformation with Addition of CeO 2 to CuO−TiO 2 System: Raman Spectroscopy, X-Ray Diffraction, and Textural Studies. *Chem. Mater.* **2002**, *14* (6), 2514–2518.
(57) Seemala, B.; Cai, C. M.; Wyman, C. E.; Christopher, P. Support Induced Control of Surface Composition in Cu–Ni/TiO 2 Catalysts Enables High Yield Co-Conversion of HMF and Furfural to Methylated Furans. *ACS Catal.* **2017**, *7* (6), 4070–4082.
(58) Larsson, P. O.; Andersson, A. Complete Oxidation of CO, Ethanol, and Ethyl Acetate over Copper Oxide Supported on Titania and Ceria Modified Titania. *J. Catal.* **1998**, *179* (1), 72–89.
(59) Biesinger, M. C.; Payne, B. P.; Lau, L. W. M.; Gerson, A.; Smart, R. S. C. X-Ray Photoelectron Spectroscopic Chemical State Quantification of Mixed Nickel Metal, Oxide and Hydroxide Systems. *Surf. Interface Anal.* **2009**, *41* (4), 324–332.
(60) Wolfbeisser, A.; Kovács, G.; Kozlov, S. M.; Föttinger, K.; Bernardi, J.; Klötzer, B.; Neyman, K. M.; Rupprechter, G. Surface Composition Changes of CuNi-ZrO2 during Methane Decomposition: An Operando NAP-XPS and Density Functional Study. *Catal. Today* **2017**, *283*, 134–143.
(61) Sinfelt, J. Catalytic Hydrogenolysis and Dehydrogenation over Copper-Nickel Alloys. *J. Catal.* **1972**, *24* (2), 283–296.
(62) Gage, S. H.; Ngo, C.; Molinari, V.; Causà, M.; Richards, R. M.; Gentile, F. S.; Pylypenko, S.; Esposito, D. Strong Metal–Support Interactions of TiN– and TiO 2 –Nickel Nanocomposite Catalysts. *J. Phys. Chem. C* **2018**, *122* (1), 339–348.
(63) Fracchia, M.; Ghigna, P.; Vertova, A.; Rondinini, S.; Minguzzi, A. Time-Resolved X-Ray Absorption Spectroscopy in (Photo)Electrochemistry. *Surfaces* **2018**, *1* (1), 138–150.
(64) Lukashuk, L.; Foettinger, K. In Situ and Operando Spectroscopy: A Powerful

Approach towards Understanding Catalysts. *Johnson Matthey Technol. Rev.* **2018**, *62* (3), 316–331.
(65) Caudillo-Flores, U.; Muñoz-Batista, M. J.; Kubacka, A.; Fernández-García, M. Operando Spectroscopy in Photocatalysis. *ChemPhotoChem* **2018**, *2* (9), 777–785.
(66) Chiarello, G. L.; Dozzi, M. V.; Scavini, M.; Grunwaldt, J.-D.; Selli, E. One Step Flame-Made Fluorinated Pt/TiO2 Photocatalysts for Hydrogen Production. *Appl. Catal. B Environ.* **2014**, *160–161*, 144–151.

Figure Captions

Figure 1

(a) SEM top-view and (b) cross-section images of 5Ni5Cu-TiO_2 NTs. (c-e) Magnified SEM top-view of as-prepared (c) 5Ni5Cu-, (d) 10Ni- and (e) 10Cu-TiO_2. (f) H_2 evolution rates for 10Ni- (blue), 5Ni5Cu- (purple) and 10Cu-TiO_2 NTs (red) measured during 4h-long photocatalytic experiments. (g-i) Magnified SEM top-view of (g) 5Ni5Cu-, (h) 10Ni- and (i) 10Cu-TiO_2 after a 4h-long photocatalytic experiment.

Figure 2

(a) XRD patterns of 10Cu- (red), 5Ni5Cu- (purple) and 10Ni-TiO_2 (blue) acquired before (solid lines) and after (dotted lines) a 4h-long photocatalytic experiment. (b) Detail of the XRD patterns in the 42-46° 2θ region. (c) Ni2p and (d) Cu2p XPS spectra for the as-prepared 5Ni5Cu-TiO_2 photocatalyst. (e) Ni2p and (f) Cu2p XPS spectra for 5Ni5Cu-TiO_2 after a 4h-long photocatalytic experiment. (g) Relative surface composition and speciation of Ni and Cu species for different samples before and after photocatalysis (determined from XPS data, for 10Ni and 10Cu see Figure S3). (h) HAADF-TEM image and (i, j) EDS-TEM maps showing the (i) Cu, Ni, Ti and (j) O elemental distribution.

Figure 3

(a) Normalized Cu K-edge XAS spectra of 10Cu- and 5Ni5Cu-TiO_2 exposed to air in the dark (standard XAS spectra of Cu, Cu_2O and CuO are reported as references) and histograms showing the Cu phase compositions. (b) Normalized Ni K-edge XAS spectra of 10Ni- and 5Ni5Cu-TiO_2 exposed to air in the dark (standard XAS spectra of Ni and NiO are reported as references) and histograms showing the Ni phase compositions. (c) Cu K-edge and (d) Ni K-edge XAS spectra of 5Ni5Cu-TiO_2 immersed in a water-ethanol solution in the cell (in the dark) for different times (5Ni5Cu-TiO_2 exposed to air in the dark is reported as reference, black curves). (e) $1-(\Delta\mu)/\mu$ values determined at 9020 eV and at 8370 eV for sample 5Ni5Cu-TiO_2 in solution for different exposure times.

Figure 4

(a) Cu K-edge and (b) Ni K-edge XAS spectra of 5Ni5Cu-TiO_2 immersed in the cell in a water-ethanol solution under UV light illumination for different exposure times; the last recorded XAS spectra for 5Ni5Cu immersed in water-ethanol solution under dark conditions are reported as reference and defines the sample condition prior to UV illumination, see black curves. (c) Cu and (d) Ni phase composition determined by operando XAS measurements for 5Ni5Cu-TiO_2 immersed in a degassed ethanol-water solution under UV light irradiation. (e) Volume of hydrogen gas evolved during a photocatalytic experiment performed using 5Ni5Cu-TiO_2. The H_2 amount was measured at different times (after 2 hours under dark conditions and after 2 and 6 hours under UV light illumination). (f) Magnified SEM top-view image of 5Ni5Cu-TiO_2-P, i.e. after photocatalysis. A few nm sized metallic NPs deposited under illumination are evidenced with purple circles.

Figures

Figure 1

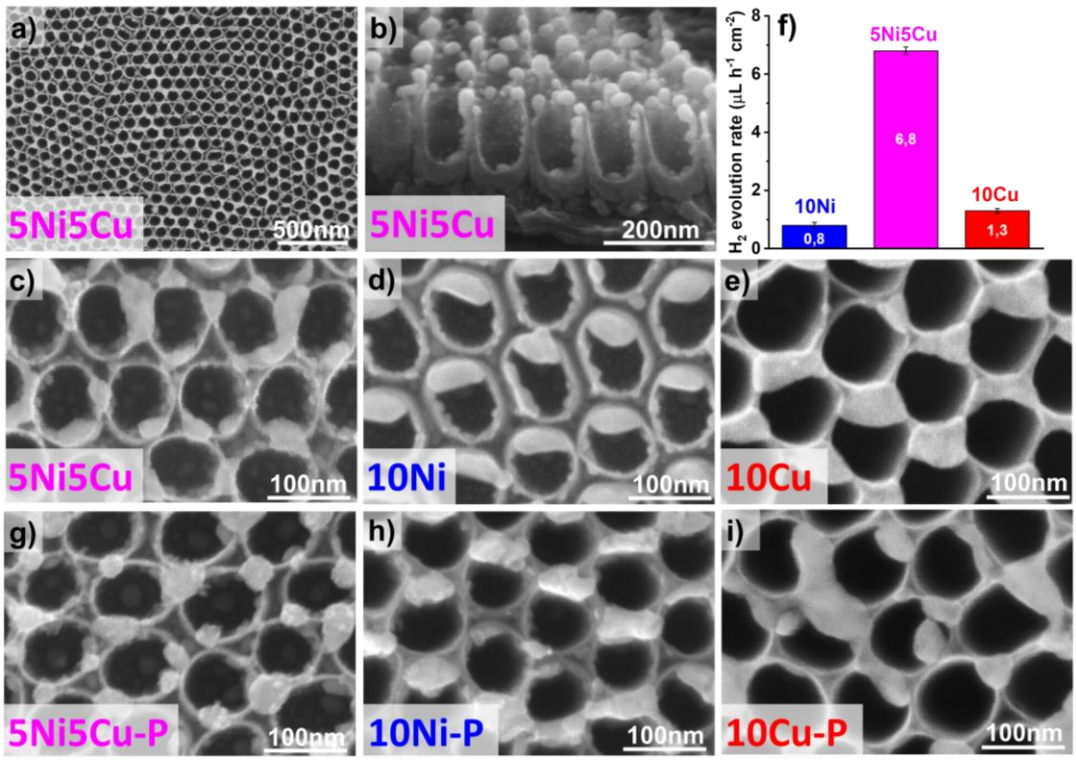

Figure 2

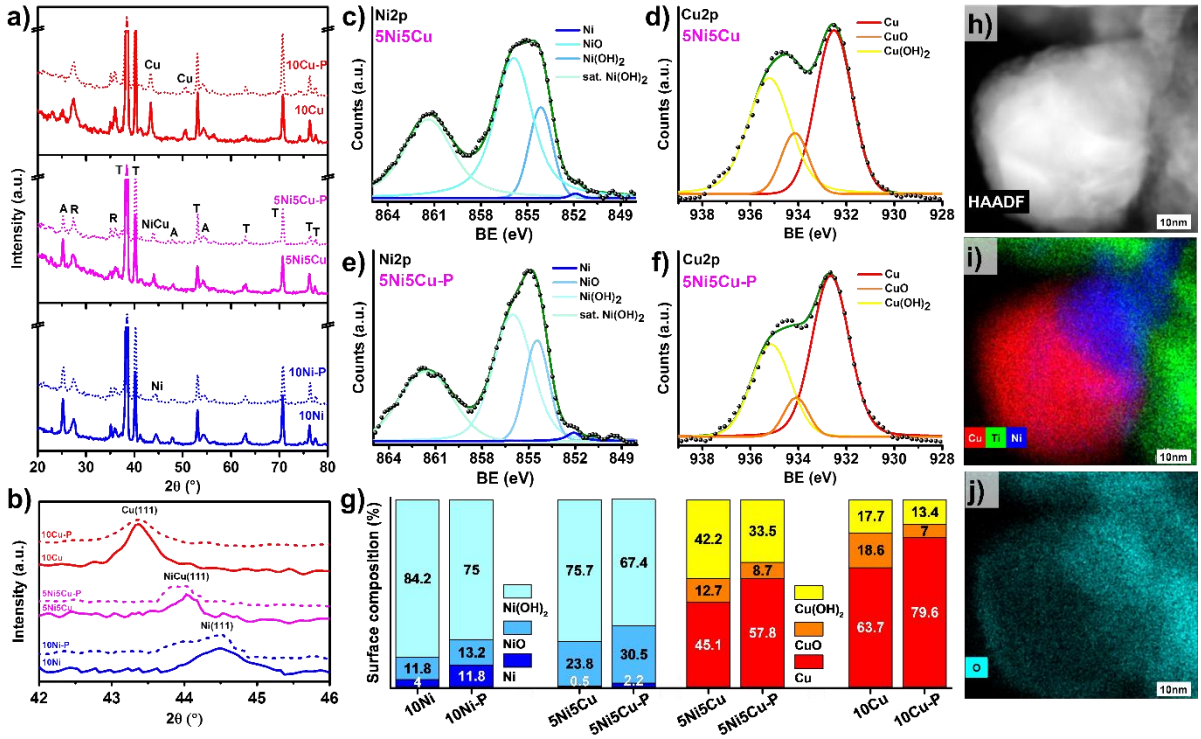
a)
Cu
Cu
10Cu-P
10Cu
T T
A R
R
NiCu
A
T
A
T
T
T T
5Ni5Cu-P
5Ni5Cu
Ni
10Ni-P
10Ni
Intensity (a.u.)
20 30 40 50 60 70 80
2θ (°)
b)
Cu(111)
10Cu-P
10Cu
NiCu(111)
5Ni5Cu-P
5Ni5Cu
Ni(111)
10Ni-P
10Ni
Intensity (a.u.)
42 43 44 45 46
2θ (°)
c)
Ni2p
5Ni5Cu
Ni
NiO
Ni(OH)2
sat. Ni(OH)2
Counts (a.u.)
864 861 858 855 852 849
BE (eV)
d)
Cu2p
5Ni5Cu
Cu
CuO
Cu(OH)2
Counts (a.u.)
938 936 934 932 930 928
BE (eV)
e)
Ni2p
5Ni5Cu-P
Ni
NiO
Ni(OH)2
sat. Ni(OH)2
Counts (a.u.)
864 861 858 855 852 849
BE (eV)
f)
Cu2p
5Ni5Cu-P
Cu
CuO
Cu(OH)2
Counts (a.u.)
938 936 934 932 930 928
BE (eV)
g)
Surface composition (%)
84.2
11.8
4
75
13.2
11.8
75.7
23.8
0.5
67.4
30.5
2.2
42.2
12.7
45.1
33.5
8.7
57.8
17.7
18.6
63.7
13.4
7
79.6
Ni(OH)2
NiO
Ni
Cu(OH)2
CuO
Cu
10Ni
10Ni-P
5Ni5Cu
5Ni5Cu-P
5Ni5Cu
5Ni5Cu-P
10Cu
10Cu-P
h)
HAADF
10nm
i)
Cu
Ti
Ni
10nm
j)
O
10nm

Figure 3

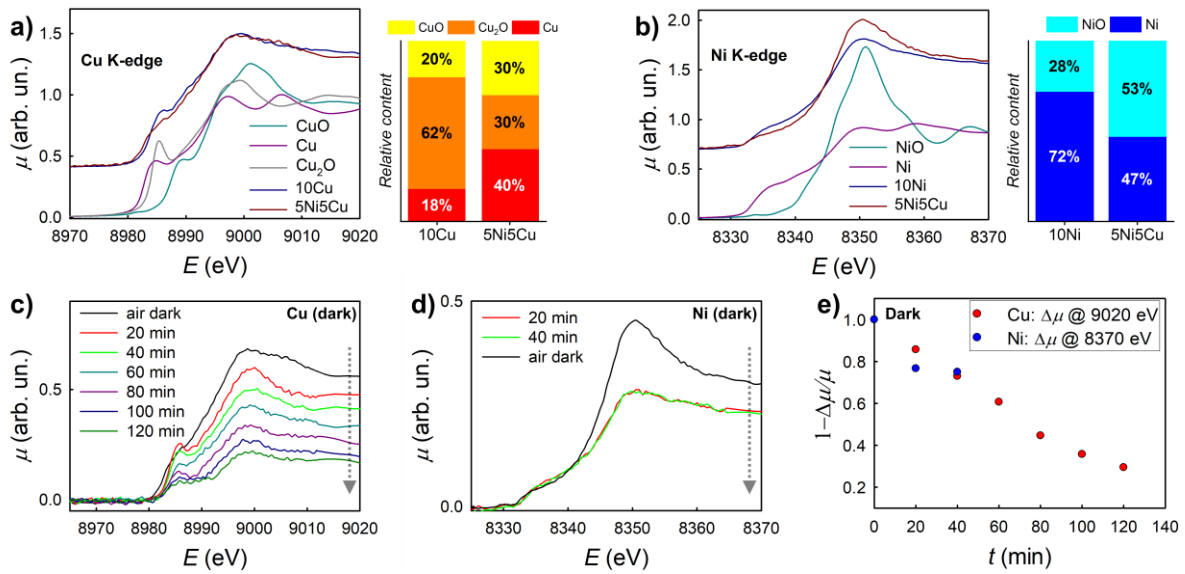
a)
Cu K-edge
μ (arb. un.)
E (eV)
CuO
Cu
Cu2O
10Cu
5Ni5Cu
Relative content
CuO
Cu2O
Cu
20%
62%
18%
30%
30%
40%
10Cu
5Ni5Cu
b)
Ni K-edge
μ (arb. un.)
E (eV)
NiO
Ni
10Ni
5Ni5Cu
Relative content
NiO
Ni
28%
72%
53%
47%
10Ni
5Ni5Cu
c)
air dark
20 min
40 min
60 min
80 min
100 min
120 min
Cu (dark)
μ (arb. un.)
E (eV)
d)
20 min
40 min
air dark
Ni (dark)
μ (arb. un.)
E (eV)
e)
Dark
Cu: Δμ @ 9020 eV
Ni: Δμ @ 8370 eV
1−Δμ/μ
t (min)

Figure 4

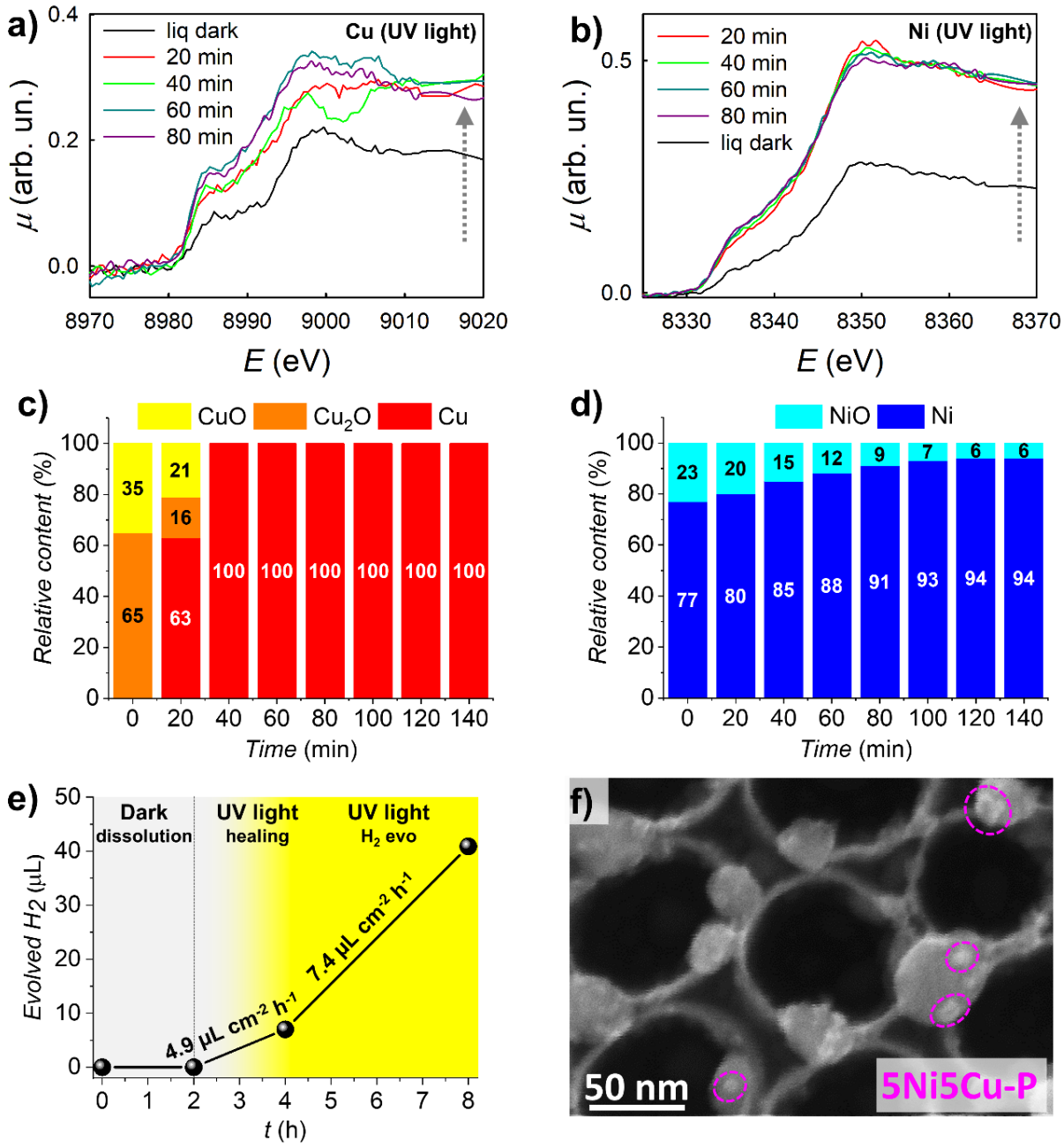
a)
Cu (UV light)
liq dark
20 min
40 min
60 min
80 min
μ (arb. un.)
E (eV)
b)
Ni (UV light)
20 min
40 min
60 min
80 min
liq dark
μ (arb. un.)
E (eV)
c)
CuO
Cu2O
Cu
Relative content (%)
Time (min)
d)
NiO
Ni
Relative content (%)
Time (min)
e)
Dark dissolution
UV light healing
UV light H2 evo
4.9 μL cm-2 h-1
7.4 μL cm-2 h-1
Evolved H2 (μL)
t (h)
f)
50 nm
5Ni5Cu-P